Chemical Engineering Communications
Publication details, including instructions for authors and subscription information:
http://www.informaworld.com/smpp/title~content=t713454788

NANOPHOSPHORS FOR WHITE LIGHT LEDS

Dongdong Jia [a]
[a] Department of Geology and Physics, Lock Haven University of Pennsylvania, Lock Haven, Pennsylvania, USA

Online Publication Date: 01 December 2007

To cite this Article Jia, Dongdong(2007)'NANOPHOSPHORS FOR WHITE LIGHT LEDS',Chemical Engineering Communications,194:12,1666 — 1687
To link to this Article: DOI: 10.1080/00986440701446359
URL: http://dx.doi.org/10.1080/00986440701446359

Chem. Eng. Comm., 194:1666–1687, 2007

ISSN: 0098-6445 print/1563-5201 online
DOI: 10.1080/00986440701446359

Taylor & Francis
Taylor & Francis Group

Nanophosphors for White Light LEDs

DONGDONG JIA

Department of Geology and Physics, Lock Haven University of Pennsylvania, Lock Haven, Pennsylvania, USA

In this article, a salted sol-gel and a salted sol-gel combustion method were developed for nanophosphor synthesis. Massive nanophosphor production becomes possible by using these novel methods. Some blue, green, and red LED nanophosphors were prepared by using these novel methods. Morphology, growth mechanism, and luminescent properties of these phosphors were investigated. Concentration quenching effect is reduced in nanophosphors. Energy transfer process is limited by increase of the surface/volume ratio. These results show that nanophosphors have great potential to enhance efficiency of phosphors, but the thermal quenching effect is increased for nanophosphors that are prepared by wet chemical methods.

Keywords Light emitting diode; Luminescence; Nanophosphor; Phosphor

Introduction

Light Emitting Diode Phosphors

Light emitting diode (LED) devices are promising solid state lighting (SSL) devices, with great potential to save electrical energy in lighting applications. Currently the lighting efficiency of LED devices is over 30 lm/W. It is expected that LED lighting efficiency will increase to over 70 lm/W by 2007 to serve as replacements for incandescent lamps and will increase to 150 lm/W by 2012 to replace fluorescent lamps. In 2020, LED lighting efficiency is expected to be over 200 lm/W (Bergh, 2003). If these goals are reached then 50% of the electrical energy currently used for lighting applications can be saved (Brodrick, 2003). But to achieve taht, there are many intermediate steps that have to be taken, for example, increasing light extraction from LED devices, improving packaging, finding better infrastructure, and discovering highly efficient LED phosphors.

There are many LEDs that emit different colors of light. UV LEDs emit near UV light from 380 to 410 nm. Blue LEDs emit blue light from 440 to 480 nm (GaN). Green LEDs emit green light from 520 to 560 nm (GaInN), and red LEDs emit red light from 590 to 630 nm (AlGaInP). But for lighting applications, white light is preferred.

For LEDs, there are several ways to generate white light. For example, using red, blue, and green LEDs together can generate white light. Using red, blue, and green phosphors to down-convert UV LED emission can also generate white light. The best method is to use yellow phosphors to convert part of the blue LED

Address correspondence to Dongdong Jia, Department of Geology and Physics, Lock Haven University of Pennsylvania, Lock Haven, PA 17745, USA

emission to generate white light. This method is also called the binary complementary method (Steigerwald et al., 2002).

To make white light LEDs, phosphors are often required for light down-conversion. These phosphors are then called LED phosphors. Energy loss during light down-conversion would reduce overall efficiency of the LED device. For this reason, many efforts have been made to search for novel, highly efficient phosphors and to improve the efficiency of the current white light LEDs. LED phosphors normally absorb strongly in the near UV or blue region to down-convert the light emitted by LEDs. Most LED phosphors are from lamp phosphors, TV phosphors, or scintillators. In general, these phosphors work better for LEDs than for fluorescent lamps because LED phosphors are exposed to low energy light (380–470 nm). For fluorescent lamps, phosphors have to be exposed to deep UV light, which can cause serious degradation (Mishra et al., 2005), but this will not happen for LED phosphors.

LED phosphors usually have broad band transitions for absorption and color rendering. Therefore, phosphors with 4f-5d transitions are good candidates. Many Eu^{2+} and Ce^{3+} related phosphors have been developed for LEDs, such as $Sr_2SiO_4:Eu^{2+}$ (Park et al., 2004), $Y_3Al_5O_{12}:Ce^{3+}$ (Schlotter et al., 1999), $SrGa_2S_4:Eu^{2+}$ (yellow, green) (Huh et al., 2003), $SrS:Eu^{2+}$ (red) (Chartier et al., 2006), and $BaMgAl_{10}O_{17}:Eu^{2+}$ (blue) (Chen et al., 2006). Some phosphors with 3d-3d transitions such as $BaMgAl_{10}O_{17}:Eu^{2+}$, Mn^{2+} are also good for LEDs (Yang et al., 2004). Absorption and emission band position of these phosphors is critical. Their absorption must be at the LED emission and their emission should meet the requirement for color rendering.

Mismatching of absorption peak of the phosphors with the LED emission can be adjusted by using a host-mixing method (Liu et al., 2006; Zhang et al., 2005). Host mixing is defined as making a solid solution of two similar ions as a new host. For example, Y^{3+} can mix with Gd^{3+}, Ca^{2+} can mix with Sr^{2+}, Mg^{2+}, or Ba^{2+}, and S^{2-} can mix with O^{2-} or Se^{2-}. Using similar ions for the solid solution can keep the perfection of the crystal structure and reduce defects that may generate traps (Jia and Yen, 2003). The 4f-5d transitions of LED phosphors are very sensitive to the host. By using host mixing, absorption peaks will have red- or blueshift to a proper position that overlaps with the LED emission. Similarly, once the absorption is matched, the emission color can also be adjusted (Hu et al., 2005).

Light Emitting Diode Nanophosphors

Nanophosphors have drawn considerable attention from scientists working on LEDs. Nanophosphor is a novel concept that was developed in early 1990s. For nanophosphors, the physics and engineering are down to a scale of 1–100 nm. Many new physics phenomena were developed for nanophosphors.

Many nanophosphors have been prepared, for example TV phosphors such as $Y_2O_3:Eu^{3+}$ (Huang et al., 2002), LED phosphors such as $Y_3Al_5O_{12}:Ce^{3+}$, and long-persistence phosphors such as $SrAl_2O_4:Eu^{2+}$, Dy^{3+}. Enhanced emission and extended persistence have been observed (Kang et al., 2003; Wang et al., 2005). One of the advantages of nanophosphors is that the internal scattering within the materials is reduced when the size of the nanophosphors is much smaller than the wavelength of the visible light (Tsao, 2002). Also, the refractive index of materials can be modified by mixing materials with different refractive indexes. The refractive

index of such a composite is close to the average of that of each component so that it is possible to engineer the refractive index of certain nanophosphor composite. A better matching of refractive index between LED and phosphor can enhance light extraction.

Luminescent intensity is also reported gain in nanocrystalline materials (Meltzer et al., 1999). When materials are in nanoscale, their surface-to-volume ratio is orders larger than that of fine powders (with a size of about 10 μm). Mixing and doping uniformity are also much better for nanophosphors than that for bulk materials during synthesis. Therefore, quality of materials, especially in term of doping uniformity and phase purity, is better and is easier to achieve (Jia et al., 2006b). As the dopants are well separated and located in each nanoparticle, the energy transfer between identical or nonequivalent emission centers, which can cause concentration quenching, is reduced due to the high surface/volume ratio (Ye et al., 1997; Jia, 2006). By their reduced size, nanophosphors can double the doping concentration without quenching effect. As a result, both absorption and emission intensities of the nanophosphors can reach much higher values. With these advantages, nanophosphors are gradually replacing traditional phosphors in many places for display, indicator, lamp, and LED applications.

Preparation of nanparticles has been studied for about 20 years. Quality of nanophosphors has been greatly improved. Methods for preparation of nanophosphors are usually wet chemical methods, including sol-gel, precipitation, coprecipitation, emulsion, combustion, and spray pyrolysis. For physical methods, ball milling is frequently used. All these methods have their own advantages and disadvantages.

Traditional wet chemical synthesis methods are very successful for preparation of nanophosphors in the laboratory. But scaleup production of nanophosphors remains a problem to be solved. For example, the conventional sol-gel method is one of the traditional wet chemical techniques that use various metal-organic (metal alkoxides) compounds as precursors to produce glass or ceramics through hydrolysis, gelation, drying, and thermal treatment processes. Precursors in the form of liquid or solutions in organic solvents are blended and mixed. However, the conventional sol-gel method is not useful for producing large amounts of phosphors because most metal alkoxides are solid and their solubility in solvents is low. For example, 100 mL of commercial yttrium isopropoxide ($Y(OC_3H_7)_3$) in toluene-isopropanol contains only the equivalent of 2 g of Y_2O_3, so production of such a phosphor is very expensive. Conventional sol-gel methods are good for simple metal oxides, but to prepare more complicated chemical compounds such as $Y_3Al_5O_{12}$(YAG), both Y_2O_3 and Al_2O_3 components have to be made separately. Mixing and sintering is required to prepare YAG. Therefore, conventional methods will require a complicated routine to make salt compounds. A more complicated process will elevate the overall cost and limit the production rate.

In this work, two novel methods for massive nanophosphor production are developed. Using these methods, the sintering temperature is lowered and the sintering time is shortened. The luminescent properties of nanophosphors prepared with these methods are investigated. For nanophosphors it is found that the concentration quenching effect is reduced and the thermal quenching effect is increased. For nanophosphors with nonequivalent emission centers, it is found that the energy transfer between nonequivalent centers is limited by a high surface/volume ratio. Some novel red nanophosphors were prepared and investigated for color rendering.

Experimental Section

Synthesis of LED Nanophosphors

In this work, synthesis of nanophosphors is a major topic. Two novel nanophosphors synthesis methods were developed and are discussed in detail in the results and discussion section. In general, these methods are wet chemical methods, the salted sol-gel method (SSG) and the salted sol-gel combustion method (SSGC). The salted sol-gel method and the salted sol-gel combustion method are developed from traditional sol-gel and combustion methods. These two methods are simple and promising methods for large-scale nanophosphor production. The equipment needed for these methods are a Jenway 1103 magnetic stirring hot plate, a tabletop box furnace ($T_{max} = 1200^{\circ}C$), and some Al_2O_3 crucibles and glass beakers.

Characterization of Morphology and Structure Properties of LED Nanophosphors

A Rigaku X-ray diffractometer was used for X-ray diffraction (XRD) to determine the structure of the nanophosphors prepared. A Philips XL30 environmental scanning electron microscope (SEM) was used to characterize the morphology of the phosphors with a size no less than 10 nm. Because all of the samples are not conductive a HUMMER IV sputter coater was used to coat Pt layers on the nanophosphors for observation. A 5 nm Pt layer was coated on each sample, which increased the SEM resolution to 10 nm so that the size and shape of the nanophosphors larger than 10 nm could be measured.

A JEOL 2010 FEG transmission electron microscope (TEM) was used for nanophosphors with a size less than 10 nm. Nanophosphors were dispersed in polymer agent and sampled for TEM measurements.

Characterization of Luminescent Properties of Nanophosphors

To characterize the luminescent properties of the nanophosphors some fundamental spectroscopy techniques were used. For emission and excitation spectra of the samples, a SPEX FluoroMax II spectrometer was used. For photoluminescence measurements, the excitation source was a Coherent INNOVA-306 argon laser. For low temperature photoluminescence measurements up to 8 K, a SPEX 1403 double spectrometer and RMC LTS-22 cryostat were used.

Results and Discussion

Synthesis, Morphology, and Structure Characterization of LED Nanophosphors

Salted Sol-Gel Method (SSG)

A novel modified sol-gel technique has been developed, called salted sol-gel technology (SSG) (Jia et al., 2006c).

In the list of metal alkoxides, many, such as aluminum sec-butoxide and gallium isopropoxide, are liquid. Some phosphor compounds contain a major composition of which the corresponding oxide can be obtained from the above list. A water solution of the other metallic salts could be prepared and blended into the liquid

alkoxides. During gelation, the water is used and the salt will be repelled and stored in the nanopores of the gel. A very uniform mixture of precursors could be obtained.

Salted sol-gel technology opens a new possibility to obtain high homogeneity of chemical composition of materials. Nanoscale homogeneous multicomponent material mixtures could be produced. Complete chemical reactions and much better crystallinity could be obtained at a much lower sintering temperatures and in a much shorter sintering period. Fine nanophosphor powders with tens to a hundred nanometer size and with good crystallinity and high efficiency could be obtained.

In addition, distribution of doping ions would be much more uniform in the sol-gel samples. Due to nonuniform distribution of doping ions, even at low doping levels, in the phosphors produced by a solid-state reaction method (SSR), local concentration could be high, and concentration quenching could appear at a low doping level. In contrast, due to higher uniformity of dopant distribution, a higher doping level may be allowed in the sol-gel derived samples. This will provide an advantage to increase absorption of UV pump light source and emit more visible light from thin coating phosphor layers by a larger number of emission centers. Thin nanophosphor coating can significantly improve the light output from lamp tubes or LED devices.

$Y_3Al_5O_{12}$:Ce (YAG:Ce) is taken as an example to demonstrate the salted sol-gel method. The YAG:Ce phosphor is widely used as a basic component for light down-conversion in current white light LED applications. To obtain YAG, Y_2O_3 and Al_2O_3 are commonly used. The melting points of Y_2O_3 and Al_2O_3 are 2410°C and 2072°C, respectively. Therefore, sintering temperature for YAG is very high. Below 1300°C, no good garnet phase can be obtained. With certain flux such as BaF_2 (20 mol%), a complete garnet phase can be formed at 1500°C.

For the SSG method, Yttrium nitrate, $Y(NO_3)_3$, or yttrium acetate, $Y(CH_3COO)_3$, are used as the salt component. They are diluted in water to make a saturated water solution at 60°C. $Ce(NO_3)_3$ is used as the doping component. The aluminum component is aluminum sec-butoxide (ASB). ASB is very moisture sensitive; reacting with water, ASB hydrolyzes to $Al(OH)_3$ and butyl alcohol. Nanopores with size around 2–10 nm are formed in the $Al(OH)_3$ gel network (Chane-Ching and Klein, 1988a, b).

ASB is soluble in isopropanol. To avoid quick hydrolysis, ASB is dissolved in isopropanol. When yttrium nitrate solution is added to ASB, hydrolysis takes place quickly. A white cloudy colloidal nanocluster suspension of $Al(OH)_3$ hydrolysis middle product immediately appears. The hydrolysis reaction of ASB with water is an exothermic reaction. Water and butyl alcohol is released during the multiple-step hydrolysis processes. The water released is recycled back into the reaction. A higher concentration of the salt solution reduces the amount of water used, which slows down the speed of hydrolysis and condensation processes and therefore limiting the growth of particle/cluster sizes. The yttrium/cerium nitrate is trapped into the $Al(OH)_3$ nanopores. Isopropanol also plays a role also as a dispersion agent. The white cloudy suspension gradually disappears after the hydrolysis process finishes, and the mixture becomes transparent. This indicates that the $Al(OH)_3$ nanoclusters are very small.

The sample gel is held at 90°C for one day. Transparent dry gel is obtained, which is a uniform mixture of Y/Ce nitrate nanoparticles within the $Al(OH)_3$ nanopores. The mixture is heated to 600°C and annealed for 2 h to decompose yttrium/cerium nitrate and aluminum hydroxides and to remove organic residuals such as butyl alcohol and isopropanol. During the annealing process the remaining

water is evaporated, leaving only the Y/Ce oxide nanoparticles in the Al_2O_3 nanopores. After that, the sample undergoes a heat treatment at 800°C for 2 h, where the YAG single phase appears. The X-ray diffraction spectrum of the sample after 800°C heat treatment is shown in Figure 1.

The YAG samples were sintered at 700°C, 800°C, 900°C, 1000°C, 1100°C, 1200°C, 1300°C, 1350°C, and 1400°C for 2 h for XRD and SEM measurements. There is a peak shift in XRD spectra for the samples sintered before reaching 1100°C, as shown in Figure 2(a). For example, the (420) peak shifts from 33.35° for the sample sintered at 800°C to 33.2° for the sample sintered at 1100°C, as shown in Figure 2(b). The peak shift is a result of size growth of the particles. Nanoparticles have a much stronger surface tension, which can usually compress the lattice to a smaller lattice constant (Noyan et al., 1997; Li et al., 2000). The (420) XRD peak angle is reduced, which means that the lattice parameters are enlarged by sintering at higher temperatures. The lattice parameters are enlarged because the particles grow bigger so that the surface tension has less compression effect on the lattice. Thus, it can be concluded that the particle size increases when sintering temperature increases. There is no peak shift after sintering at 1100°C, which shows that the size growth is stopped at 1100°C.

A higher sintering temperature usually generates better crystalline materials. As a result, XRD peaks are stronger and sharper for samples sintered at a higher temperature. When the XRD peak stops growing, it usually means that the reaction is complete and the best crystalline has been reached. For the SSG samples, the (420) XRD peak intensity reaches maximum at about 1350°–1400°C, indicating that the complete YAG phase is achieved at about 1350°C, as shown in Figure 3(a). In Figure 3(b), relative luminescence intensity of the SSG samples sintered at different temperatures is shown. For comparison, similar results for YAG:Tb prepared by using the SSR method with and without flux BaF_2 are also shown in the figure

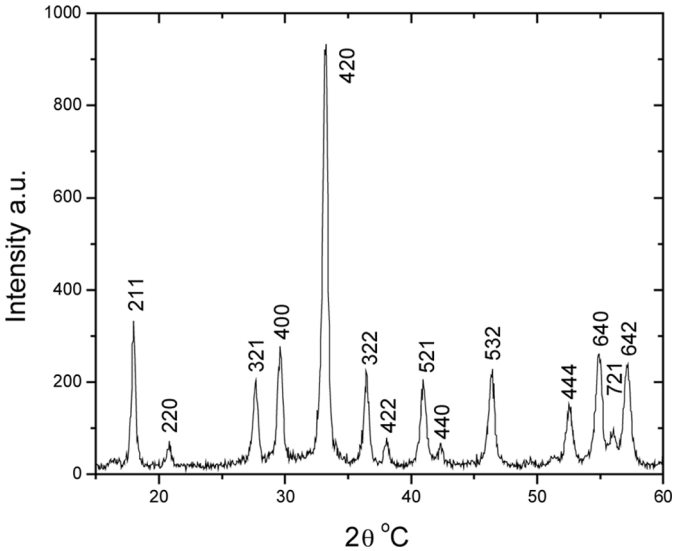

Figure 1. XRD pattern of the SSG YAG sample sintered at 800°C for 2 h.

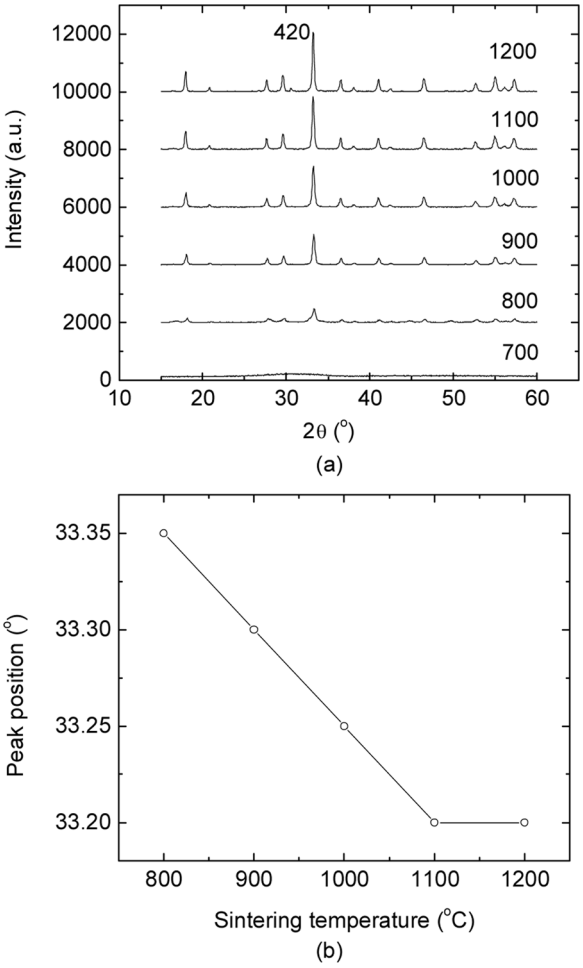

Figure 2. (a) XRD spectra of the SSG samples sintered at different temperatures for 2 h; (b) (420) peak shift with sintering temperatures.

(Ohno and Abe, 1986). It can be seen that samples created by the SSG method show lower sintering temperatures, at which samples give the strongest luminescence.

SEM images were taken with the samples first annealed at 600°C for 2 h and then sintered at 900°C for 2 h, as shown in Figure 4. The morphology of YAG samples is conglomerates. From the SEM image the particle sizes of YAG conglomerates are estimated to be between 30 and 60 nm. The aggregation of YAG nanoparticles is due to the nature of a sol-gel preparation.

Salted Sol-Gel Combustion Method (SSGC)

The sol-gel combustion method is a combination of the sol-gel method and the combustion method. Fuels such as glicin and triethanolamine (TEA) are mixed with sol-gel precursors (Chander et al., 2004; Peng et al., 2004). During the sol-gel process, the fuels are properly mixed with the gel and the trapped salts. Therefore, during

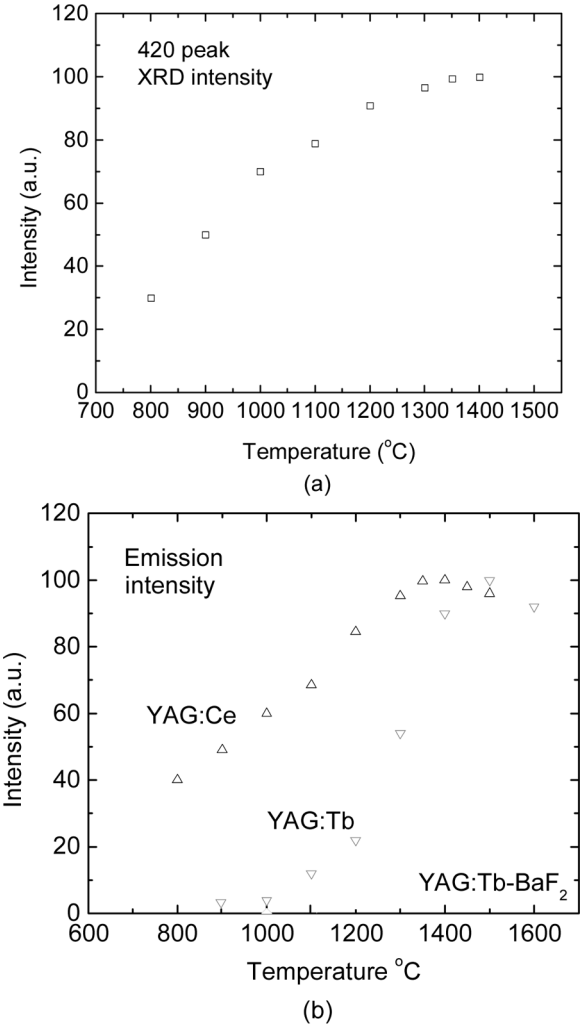

Figure 3. (a) 420 peak XRD intensity at different sintering temperatures; (b) luminescent emission intensity as a function of heat treatment temperature. Upward pointing triangles: SSG YAG:Ce sample; downward pointing triangles: SSR YAG:Tb sample with BaF_2 flux; open diamonds: SSR YAG:Tb sample without flux (Ohno and Abe, 1986).

combustion, all of the components in the mixture are broken to nanoparticles, with very good uniformity instead of clusters.

As an example, YAG:Ce was prepared by using this technique. $Y(CH_3COO)_3$ and $Al(NO_3)_3$ were used as synthesis components. They were dissolved in distilled water together with $Ce(NO_3)_3$ as a dopant component. TEA was added and mixed as a fuel. The solution was heated to 75°C to distill out the water content slowly. A small amount of ethyl glycol (EG) was added to the mixture to set the pH below 5 in order to obtain an oxide gel instead of a hydroxide gel.

When the water was almost totally distilled out, the wet solution was put at 105°C in an oven. The remaining water was boiled quickly. As the water totally dried

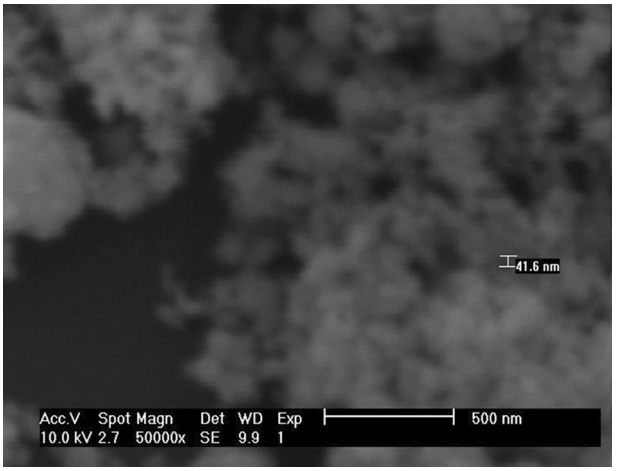

Figure 4. SEM images of SSG YAG:Ce sample sintered at 900°C.

out, a puffy brown color dry gel was obtained. The dry gel is a mixture of yttrium acetate-aluminum nitrate-glycolate porous gel network and traps TEA fuel within the nanopores. The dry gel was then ground and put in a furnace to heat to 300°C. The TEA fuel started to ignite and burn at 295°C. A dark grey puffy solid was obtained. The puffy solid was ground in an agate mortar and annealed at 600°C for 2 h in a furnace to decompose yttrium acetate and aluminum nitrate and to burn out the residual organics. White powder of Y_2O_3 and Al_2O_3 mixture was then obtained. The mixture was sintered at 800°C for 2 h to obtain YAG phase, as shown in the XRD spectrum in Figure 5.

An SEM image of YAG:Ce prepared with the salted sol-gel combustion method is shown in Figure 6. The sample was annealed at 600°C for 2 h and sintered at 800°C

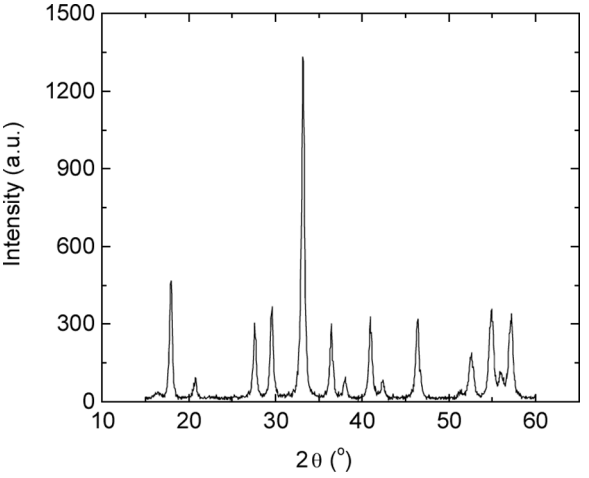

Figure 5. XRD spectrum of SSGC YAG:Ce sample. The sample was annealed at 600°C for 2 h and sintered at 800°C for 2 h.

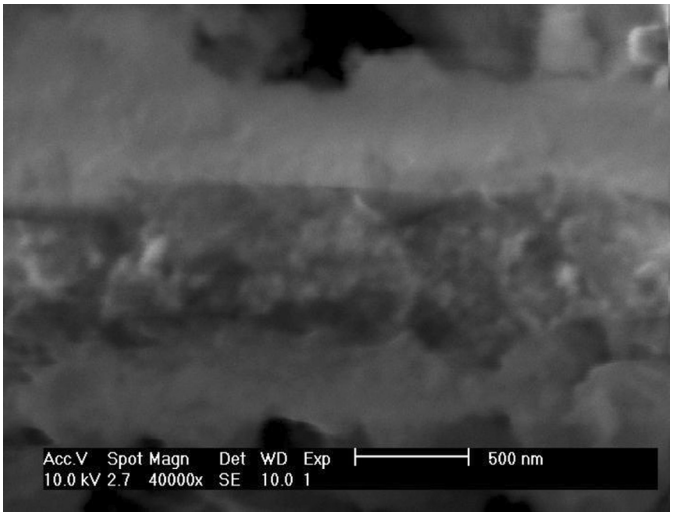

Figure 6. SEM image of the conglomerates of SSGC YAG:Ce sample. Sample was coated with 5 nm of Pt for conductivity.

for 2 h. Aggregation of nanophosphors made the sample appear as conglomerates. The size of the conglomerates is about 30–50 nm. The conglomerates can be separated by using the polymer dispersion method. After the nanophosphors were dispersed with isopropanol, TEM images were taken for the same sample. The TEM images are shown in Figure 7. The results reveal that YAG nanophosphors have a size from 5 to 10 nm. Similar results were also obtained for $Sr_4Al_{14}O_{25}:Eu^{2+}$ (SAO) and $BaMgAl_{10}O_{17}:Eu^{2+}$ (BAM) UV LED phosphors.

Optical Characterization of Nanophosphors

Luminescence Property of YAG:Ce

Yttrium aluminum garnet doped with Ce^{3+} (YAG:Ce) is one of the most important LED phosphors for white light LEDs. The emission and excitation spectra of YAG:Ce^{3+} are shown in Figure 8. A broad emission band peaking at 530 nm with a shoulder at 560 nm is due to Ce^{3+} 5d to 4f ($^2F_{5/2,7/2}$) transitions. The excitation peaks are broad bands located at blue 460 nm and UV 340 nm, which are assigned to the field splitting 5d levels. The emission and absorption peaks of YAG:Ce usually vary with synthesis methods, sizes, doping concentrations, and other factors. This is because the 4f-5d transitions of Ce^{3+} are very sensitive to the host environment (Dorenbos, 2000).

To optimize YAG:Ce quality, various synthesis methods are used, such as the SSR, SSG, and SSGC methods.

YAG phosphors are usually synthesized by using the SSR method with a flux such as BaF_2 or B_2O_3. Both of BaF_2 and B_2O_3 are insoluble in water. The flux content is generally not welcome for various reasons. Since it is hard to get rid of BaF_2 and B_2O_3, other flux is preferred. For the SSR method, new fluxes, PbO (with SiO_2 or Ta_2O_5 for charge compensation) and CsCl, were used. The melting points of PbO and CsCl are at 886°C and 645°C, respectively. A Pb ion can replace a Y ion in the

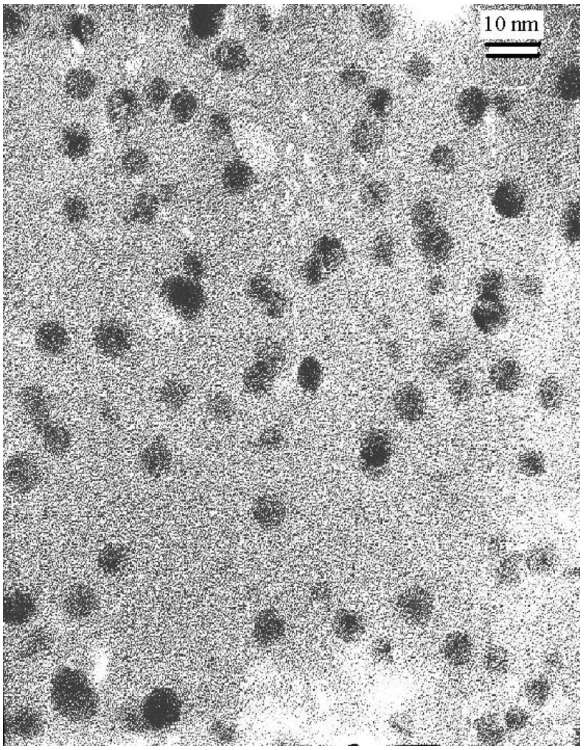

Figure 7. TEM image of the SSGC YAG sample, sintered at 800°C (bar inside = 10 nm).

YAG lattice, hence it is not necessary to remove Pb flux from the final product. A Cs ion is too large to enter the YAG lattice so it will be left out of the YAG lattice. But CsCl is soluble in water so that CsCl can be easily washed out with water from the

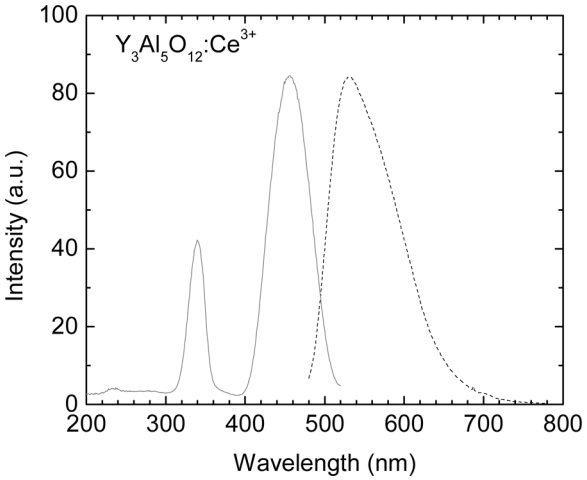

Figure 8. Emission and excitation spectra of SSG YAG:Ce sample.

final product. For the above reasons, PbO and CsCl were considered as replacements for BaF_2 and B_2O_3.

For the SSR method, Ce doping concentration was set at 2%, which is the best concentration for room-temperature emission (Murakami, 1999; Ninagawa et al., 1971). For the SSG method, the best doping concentration is about 4%. For the SSGC method the best concentration is about 2–3%. All four samples were sintered at 1350°C for 2 h with reducing gas.

Emission spectra of all four samples are shown in Figure 9. All curves were normalized to the SSR-PbO sample emission. It was found that for the SSG method with 4% doping concentration the emission intensity was about 20% stronger than that of the SSR-PbO sample. For the SSGC method, the emission was about 14% better than that of the SSR-PbO sample. For the SSR-CsCl sample, the emission intensity was about same as that of the SSR-PbO sample.

It was reported that when the size of phosphors was reduced to nanoscale, energy transfer between equivalent and nonequivalent emission centers was reduced considerably because of the high surface/volume ratio. Energy transfer between two ions cannot take place if they are in different lattices. Therefore, a high surface (interface)/volume ratio will isolate the emission ions. For this reason, doping concentration is higher than that of the bulk materials (Ye et al., 1997).

YAG:Ce samples were prepared with different doping concentrations of Ce^{3+} from 0.2% to 20% ($Y_{3-x}Al_5O_{12}$:xCe) by using the SSG method. Samples were sintered at 1350°C for 2 h with reducing gas flow to reduce Ce^{4+} to Ce^{3+} before optical measurement. Emission and excitation spectra of all samples were measured. Maximum emission intensity at each concentration was found by pumping the samples at their maximum excitation wavelength. The concentration-dependent luminescent intensity of YAG:Ce prepared with the SSG method is shown in Figure 10. The best concentration from Figure 10 is about 4%.

Peak wavelength of YAG:Ce emission also showed concentration dependence. The emission peak wavelength increased from 527 nm at 0.2% to 551 nm at 12%,

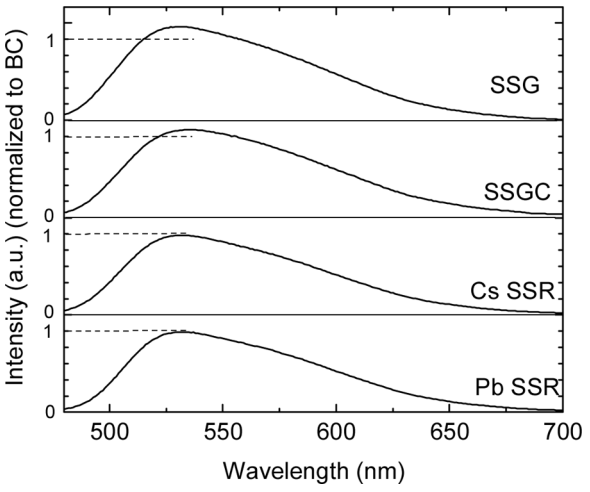

Figure 9. Emission spectra of YAG samples prepared by using Pb (SSR) with PbO as flux, Cs (SSR) with CsCl as flux, SSG method, and SSGC method.

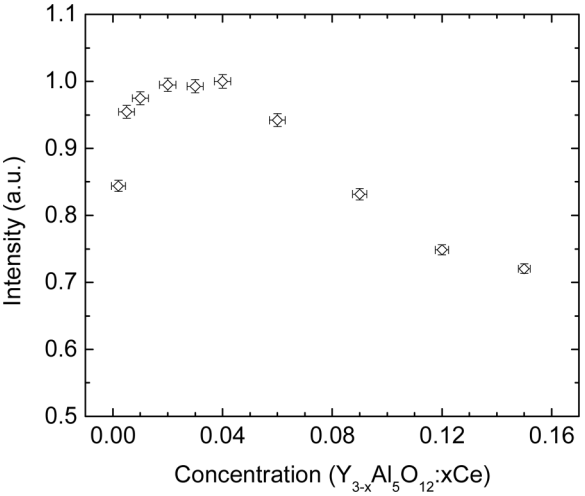

Figure 10. Concentration-dependent luminescence intensity of SSG YAG:Ce sample.

as shown in Figure 11. The wavelength change with concentration is generally due to ligand field dependence of 4f-5d transition. In the case of doping Ce^{3+} into YAG, the Ce^{3+} ions will substitute the Y^{3+} ions for the same valence state. A Y^{3+} ion has an ionic radius of only 1.019 Å in the eight-fold coordinates, while a Ce^{3+} ion has an ionic radius of 1.283 Å in the eight-fold coordinates. A lattice expansion would be expected at each doping concentration. A higher doping concentration will induce a larger lattice parameter increase. An expanded lattice will reduce the ligand field and hence will result in a redshift of emission and excitation peaks of the Ce^{3+} 4f-5d transitions.

Luminescence intensity of the 4% sample prepared by using the SSG method and the 2% sample prepared by using the SSR method was measured at different

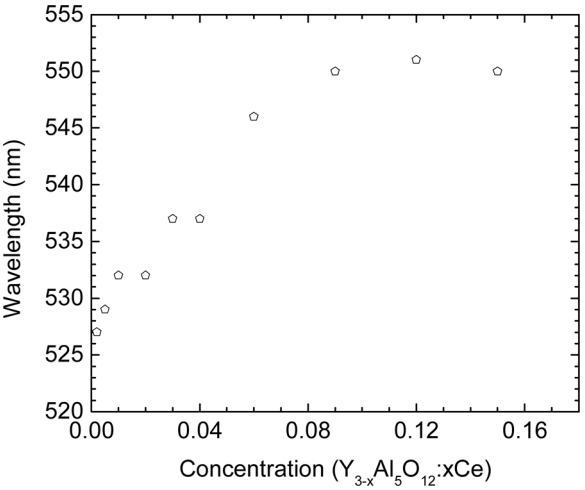

Figure 11. Redshift of emission peaks with doping concentration.

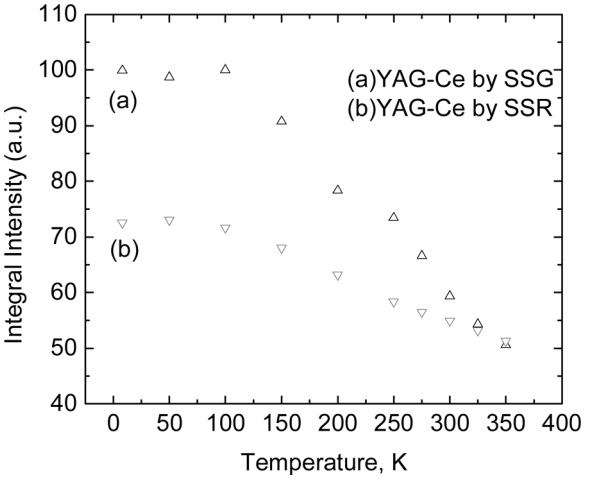

Figure 12. Temperature dependence of luminescence intensity: (a) 4% sample by SSG, (b) 2% sample by SSR.

temperatures from 8 to 350 K. The temperature dependence of luminescence intensity for the two samples is shown in Figure 12. Emission intensity started to drop quickly at about 100 K for both samples. This indicates that the onset thermal quenching temperature should be at 100 K. The emission of the SSG sample dropped much quicker than that of the SSR sample, indicating that the thermal quenching effect is stronger for the sample prepared with the SSG method. The reason can be the OH^- residual from the $Al(OH)_3$ middle product and water content. The OH^- was one of the major luminescence killers for sol-gel samples (Silversmith et al., 2006). For the wet chemical synthesis method, how to remove organic residuals is one of the major concerns. At temperatures below 100 K, the 4% SSG sample was more than 40% stronger than the 2% SSR sample, but it became only 20% stronger at room temperature.

Energy Transfer between Nonequivalent Centers in $Sr_4Al_{14}O_{25}:Eu^{2+}$

White light UV LEDs are less attractive than white light blue LEDs. One of the obvious reasons is that down-conversion of UV LED photons to blue, green, and red photons wastes more photo energy than down-conversion of blue LED photons to yellow and red photons. But, UV LED phosphors are still candidates for white light sources. $Sr_4Al_{14}O_{25}:Eu^{2+}$ is one of the traditional lamp phosphors. It can be used as the blue component for UV LEDs. By using the SSG method, nanofiber $Sr_4Al_{14}O_{25}:Eu^{2+}$ can be synthesized as shown in Figure 13. The diameter of the nanofiber is about 10–20 nm.

Similar to YAG, $Sr_4Al_{14}O_{25}:Eu^{2+}$ is very hard to obtain. By using the SSR method with a flux, a good $Sr_4Al_{14}O_{25}:Eu^{2+}$ phase can be obtained at 1300°C (Kamiya and Mizuno, 1999; Nag and Kutty, 2000). By using the SSG method, $Sr_4Al_{14}O_{25}:Eu^{2+}$ can be obtained at 900°C for 2 h sintering, as shown in Figure 14.

$Sr_4Al_{14}O_{25}$ has an orthorhombic P_{mam} space group with $a = 24.785$, $b = 4.866$, and $c = 8.487$ Å. It is built with alternating planes containing both AlO_6 octahedral and AlO_4 tetrahedral structures. Two mirror symmetry planes are formed. Sr^{2+} has

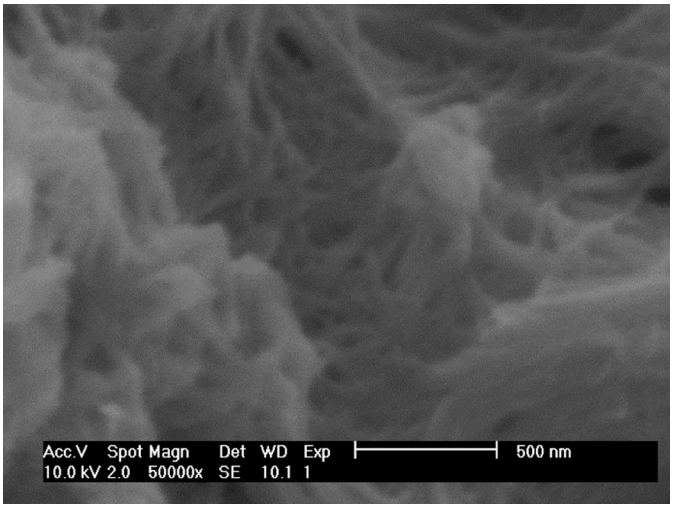

Figure 13. $Sr_4Al_{14}O_{25}:Eu^{2+}$ nanofiber obtained by sintering at 900°C for 2 h.

two sites with Sr–O distances of 2.58 and 2.74 Å. Eu^{2+} ions stay in both Sr^{2+} sites. Strong energy transfer between the two nonequivalent Eu^{2+} centers has been reported (Smets et al., 1989).

Emission peaks of the SSG samples were found at 408 nm and 487 nm under UV excitation respectively, as shown in Figures 15(a) and (c). These emission peaks correspond to the Eu^{2+} $4f^6 5d^1$ to $4f^7$ transitions at two different Eu^{2+} sites. The excitation spectra measured by monitoring at 408 nm and 487 nm emission are shown in Figure 15(a) and (c). The 5d state slitting is found to be stronger for the 487 nm site than that for the 408 nm site, so that the 487 nm site should have a shorter Eu-O distance.

For comparison, $Sr_4Al_{14}O_{25}:Eu^{2+}$ was also prepared with the SSR method. B_2O_3 was used as a flux. The samples were sintered at 1350°C for 2 h. The Eu^{2+}

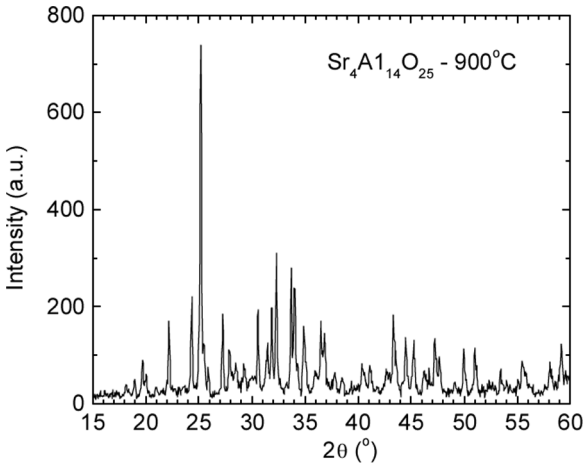

Figure 14. XRD spectrum of SSG sample sintered at 900°C.

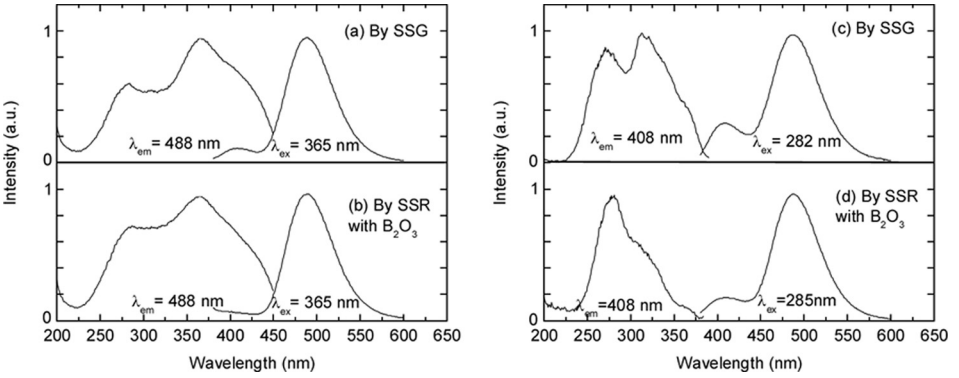

Figure 15. Emission and excitation spectra of the $Sr_4Al_{14}O_{25}$ samples: (a) excitation ($\lambda_{em} = 488$ nm) and emission ($\lambda_{ex} = 365$ nm) spectra of SSG sample; (b) excitation ($\lambda_{em} = 488$ nm) and emission ($\lambda_{ex} = 365$ nm) spectra of SSR sample, (c) excitation ($\lambda_{em} = 408$ nm) and emission ($\lambda_{ex} = 282$ nm) spectra of SSG; (d) excitation ($\lambda_{em} = 408$ nm) and emission ($\lambda_{ex} = 285$ nm) spectra of SSR sample.

luminescence from two sites was also found in the SSR samples, as shown in Figures 15(b) and (d). In Figure 15(b), the 408 nm emission peak did not appear because of the energy transfer between nonequivalent Eu^{2+} centers. Comparing the emission spectra in Figure 15(a) and Figure 15(c) to those in Figure 15(b) and Figure 15(d), it can be easily seen that in the SSG sample only 46% of the Eu^{2+} at the 408 nm site transferred its energy to the 487 nm site, and in the SSR sample, about 99.2% of the Eu^{2+} at the 408 nm site transferred its energy to the 487 nm site, under 365 nm excitation (main absorption for the 487 nm site). Under deeper UV excitation (main absorption for the 408 nm site), only 35% and 93.5% of Eu^{2+} transferred their energy to the other site in the SSG and the SSR samples respectively. There was a stronger energy transfer in the SSR samples than in the SSG sample that can be found in excitation spectra. Comparing excitation spectra monitored at 408 nm in Figure 15(c) to Figure 15(d), a weaker energy transfer in the SSG sample gave a considerable amount of rise (55%) of the excitation peak at 316 nm. A similar rise can be also found in Figure 15(a) and 15(b) around 316 nm.

It has been reported that energy transfer between nonequivalent Eu^{2+} centers occurred at a Eu^{2+} concentration above 1% (Blasse, 1986). The probability of energy transfer from $|Eu_1^*, Eu_2>$ state to $|Eu_1, Eu_2^*>$ state $P_{Eu1-Eu2}$ is given by (* is used to denote that the Eu^{2+} ion is at the excited state, and Eu_1 and Eu_2 are Eu sites at 408 nm and 487 nm respectively):

$$P_{Eu1\text{-}Eu2} = 2\pi/h|<Eu_1^*, Eu_2|H_{Eu1-Eu2}|Eu_1, Eu_2^*>|^2 \int F_{Eu1}(E) * F_{Eu2}(E)dE$$

where $H_{Eu1-Eu2} = (1/4\ \pi\varepsilon_o)\ (1/\kappa)\ \Sigma_{i,j}(e^2/|R + r_{Eu1j} - r_{Eu2i}|)$ is the electrostatic interaction between Eu ions in different sites, h is Planck's constant, and $F_{Eu1}(E)$ and $F_{Eu2}(E)$ are the line functions for the two Eu emissions. $P_{Eu1\text{-}Eu2}$ should be proportional to R^6 where R is the distance between Eu^{2+} ions. An estimate of R was found that R must be 3–4 nm for energy transfer to be sufficient (Jia et al., 2001). This yielded a critical concentration around 1% for an average Eu-Eu distance of about R = 3 nm. Therefore for 1% Eu doping, energy transfer from Eu_1 to Eu_2 is

sufficient. It was found that more than 95% of Eu 408 nm emission was transferred to Eu 487 nm emission, which agreed with our results for the SSR sample.

In the case of the SSG sample, the energy transfer rates were just about 30–50% of the SSR sample. This low energy transfer rate can be explained by its nanoscale nature. We expected that there will be no or much weaker energy transfer if the nonequivalent Eu^{2+} ions are located in two different lattices. The SSG sample has a diameter of about 10–20 nm so that it is very much a one-dimensional structure compared to the average 3–4 nm critical distances for energy transfer to take place. Therefore, the energy transfer rate drops considerably due to a smaller cross section.

BAM Blue LED Nanophosphors

$BaMgAl_{10}O_{17}:Eu^{2+}$ (BAM) is a phosphor used for plasma display panels (PDP). It can also be used as a blue component for white light UV LEDs. In this work, BAM samples were prepared with the SSG, SSGC, and SSR methods with 1% of Eu^{2+} doping concentration. For the SSG sample, barium acetate and magnesium acetate were dissolved in water together with 1% of $EuCl_3$. The solution was mixed with ASB for hydrolyzation. The gel was dried at 80°C and was annealed at 600°C for 2 h. The XRD spectra indicated that the BAM phase can be obtained by sintering the samples at 900°C for 2 h, as shown Figure 16. For the SSGC method, barium acetate, magnesium acetate, and aluminum nitrate were dissolved in water with 1% of $EuCl_3$. The solution was mixed with a TEA fuel. The gel was obtained at 110°C and was combusted at 300°C. The annealing of sample was at 600°C for 2 h. Similar to the SSG method, after the sample is sintered at 900°C for 2 h the BAM phase can be obtained, as shown in Figure 16. A BAM sample was also obtained by using the SSR method. Barium acetate, magnesium acetate, and aluminum nitrate were mixed with 1% of $EuCl_3$. B_2O_3 was used as a flux. The mixture was sintered at 1350°C for 5 h.

All samples were reduced at 1350°C for 2 h before any optical measurement. Emission and excitation spectra of all three samples were obtained and are shown

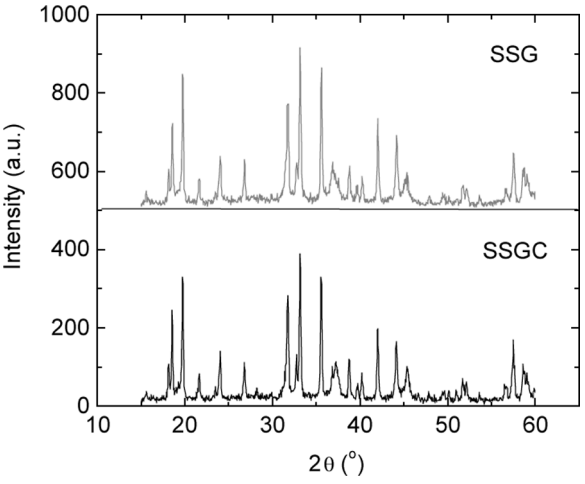

Figure 16. XRD spectra of BAM prepared by SSG and SSGC methods (β-alumina structure, space group $P_{63/mmc}$).

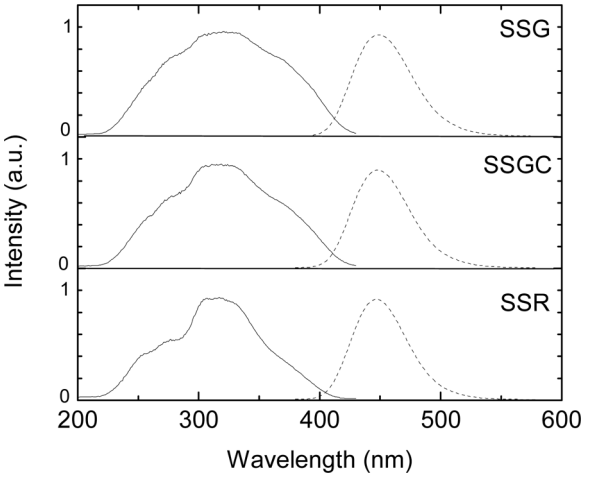

Figure 17. Emission and excitation spectra of BAM samples.

in Figure 17. The emission peak was found at 450 nm and excitation peaks were in UV. The emission peaks were almost identical, while the excitation peaks were similar to each other but showed some distortions. The emission intensity was almost identical for the three samples when they were excited at the main excitation peak 320 nm.

Alkali Earth Silicate Red LED Nanophosphors

For a white light LED, using either UV or blue LEDs, color rendering is needed. Red-emitting phosphors are important components for color rendering. Several red phosphors were investigated in this work. For example, $Ca_2ZnSi_2O_7:Eu^{2+}$ with a hardystonite structure (Haussuhl and Liebertz, 2004) is a novel red-emitting

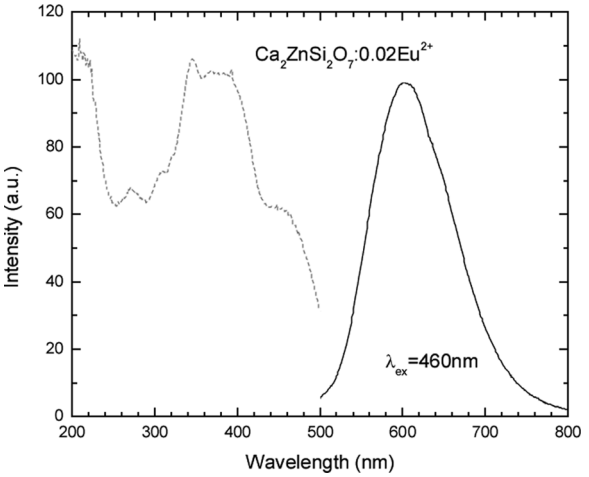

Figure 18. Emission and excitation spectra of $Ca_2ZnSi_2O_7:Eu^{2+}$.

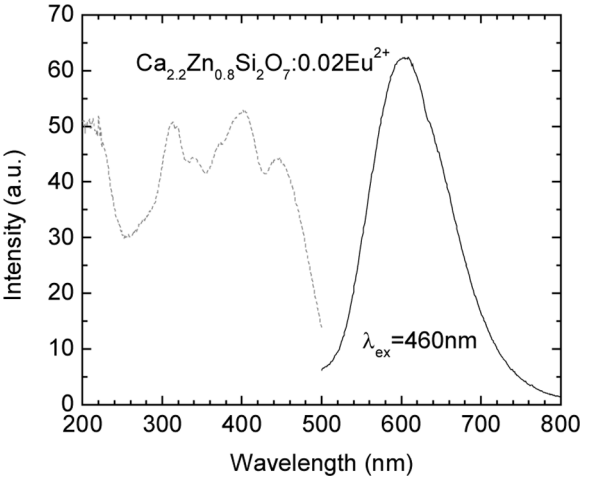

Figure 19. Emission and excitation spectra of $Ca_{2.2}Zn_{0.8}Si_2O_7:Eu^{2+}$.

phosphor that was reported recently (Jia et al., 2006a). Its emission peak is at 610 nm and its excitation maximum is at 370 nm with a shoulder at 460 nm, as shown in Figure 18.

The emission spectrum is just about what is needed for color rendering but the excitation spectrum should be further moved to 460 nm for blue LED pumping. To achieve that, zinc content was reduced and calcium content was increased. The sample prepared by the SSG method was sintering at 1100°C for 2 h in $N_2 + 5\%H_2$ to reduce Eu^{3+} to Eu^{2+}. Emission and excitation spectra of the samples are shown in Figures 19 and 20. It was found that the wavelength of the emission experienced a blueshift from 610 nm to 605 nm to 600 nm as the content of $x = 0$, 0.2, and 0.5 in $Ca_{2+x}Zn_{1-x}Si_2O_7:Eu^{2+}$ respectively, which is good for color rendering. Meanwhile, the excitation spectrum blueshifted to 460 nm. A Ca^{2+} ion has about 1 Å radius and

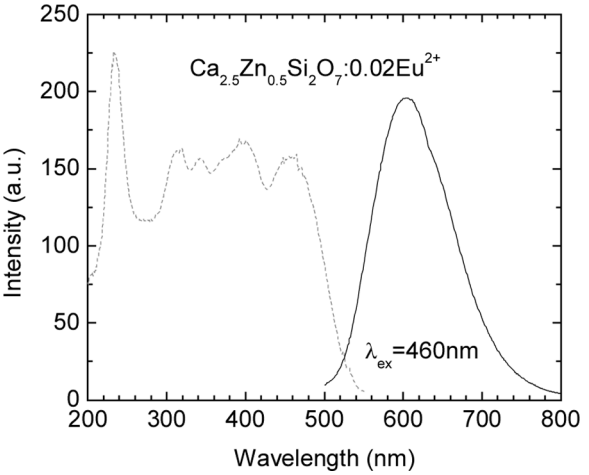

Figure 20. Emission and excitation spectra of $Ca_{2.5}Zn_{0.5}Si_2O_7:Eu^{2+}$.

a Zn^{2+} ion has about 0.6 Å radius. Increasing larger ion content in the crystal lattice will result in a lattice expansion, hence the ligand field is reduced. Since there will be a weaker 5d level splitting in a weaker ligand field, blue- and redshift were observed for emission and excitation respectively.

Conclusion

A novel salted sol-gel (SSG) method, salted sol-gel combustion (SSGC) method, and stabilized precipitation (SP) method were developed to prepare LED nanophosphors. Using a salt solution to replace water in a sol-gel process could achieve very uniform nanoscale mixing. The grain size of the raw materials in a gel mixture is less than 10 nm. Thus the sintering temperature for complete reaction is only about 800–900°C for YAG, $Sr_4Al_{14}O_{25}$, and BAM materials, which are usually required to be sintered above 1300°C with a flux.

Blue (BAM:Eu and $Sr_4Al_{14}O_{25}$:Eu), green (YAG:Ce), and red ($Ca_2ZnSi_2O_7$:Eu) nanophosphors were prepared with the novel methods. Their optical properties are better or the same as the bulk materials. Concentration quenching and energy transfer were found reduced by an increase of surface/volume ratio in nanophosphors.

References

Bergh, A. A. (2003). *A View on the Future of Solid State Lighting*, Optoelectronics Industry Development Association, Washington, D.C.

Blasse, G. (1986). Energy-transfer between inequivalent Eu^{2+} ions, *J. Solid State Chem.*, **62**, 207.

Brodrick, J. R. (2003). *DOE Solid State Lighting Status and Future*, U.S. Dept. of Energy, Office of Energy Efficiency and Renewable Energy. http://www.netl.doe.gov/ssl/PDFs/DOE%20SPIE%20Presentation%20080304.pdf

Chander, H., Haranath, D., Shanker, V., and Sharma, P. (2004). Synthesis of nanocrystals of long persisting phosphor by modified combustion technique, *J. Cryst. Growth*, **271**, 307.

Chane-Ching, J.-Y. and Klein, L. C. (1988a). Hydrolysis in the aluminum sec-butoxide water isopropyl-alcohol system 1. Rheology and gel structures, *J. Am. Ceram. Soc.*, **71**, 83.

Chane-Ching, J.-Y. and Klein, L. C. (1988b). Hydrolysis in the aluminum sec-butoxide water isopropyl-alcohol system. 2. Aging and microstructure, *J. Am. Ceram. Soc.*, **71**, 86.

Chartier, C., Barthou, C., Benalloul, P., and Frigerlo, J. M. (2006). Bandgap energy of $SrGa_2S_4$:Eu^{2+} and SrS:Eu^{2+}, *Electrochem. Solid State Lett.*, **9**, G53.

Chen, L., Sun, I., Hwang, C., and Chang, S. (2006). Luminescence properties of BAM phosphor synthesized by TEA coprecipitation method, *J. Lumin.*, **118**, 293.

Dorenbos, P. (2000). The 4fn?4fn?15d transitions of the trivalent lanthanides in halogenides and chalcogenides, *J. Lumin.*, **91**, 91.

Haussuhl, S. and Liebertz, J. (2004). Elastic and thermoelastic properties of synthetic $Ca_2MgSi_2O_7$ ((a) over-circleakermanite) and $Ca_2ZnSi_2O_7$ (hardystonite), *Phys. Chem. of Miner.*, **31**, 565.

Hu, Y., Zhuang, W., Ye, H., Zhang, S., Fang, Y., and Huang, X. (2005). Preparation and luminescent properties of (Ca1-x, Srx) S:Eu^{2+} red-emitting phosphor for white LED, *J. Lumin.*, **111**, 139.

Huang, H., Xu, G. Q., Chin, W. S., Gan, L. M., and Chew, C. H. (2002). Synthesis and characterization of Eu:Y_2O_3 nanoparticles, *Nanotechnology*, **13**, 318.

Huh, Y., Shim, J., Kim, Y., and Do, Y. R. (2003). Optical properties of three-band white light emitting diodes, *J. Electrochem. Soc.*, **150**, H57.

Jia, D. D. (2006). $Sr_4Al_{14}O_{25}:Eu^{2+}$ nanophosphor synthesized with salted sol-gel method, *Electrochem. Solid State Lett.*, **9**, H93.

Jia, D. and Yen, W. M. (2003). Trapping dynamics associated with delocalization and tunneling of Ce^{3+} doped $CaAl_2O_4$: A persistent phosphor, *J. Electrochem. Soc.*, **150**(H61), 505.

Jia, D. D., Zhu, J., Wu, B., and E, S. (2001). Luminescence and energy transfer in $CaAl_4O_7:Tb^{3+}$, Ce^{3+}, *J. Lumin.*, **93**, 107.

Jia, D. D., Goonewardene, A., Jia, W., Guo, X., Zou, Y. K., and Li, K. (2006a). Sulfide Phosphors for LED white light sources, Paper presented at Materials Research Society Spring meeting, San Francsico.

Jia, D. D., Wang, Y., Guo, X., Li, K., Zou, K., and Jia, W. (2006b). Synthesize and Characterize YAG:Ce^{3+} LED Nanophosphor, *J. Electrochem. Soc.*, **154**, J1.

Jia, D., Weyant, J. E., Shaffer, C. V., Goonewardene, A., Wang, Y., Guo, X., Li, K., Zou, K., and Jia, W. (2006c). YAG:Ce^{3+} Nanophosphor synthesized with salted sol-gel method, *Nanotechnology*, **1**, 339.

Kamiya, S. and Mizuno, H. (1999). Classification of fluorescent lamps by chromaticity and color rendering properties, in: *Phosphor Handbook*, eds. S. Shionoya and W. M. Yen, CRC Press, Boca Raton, Fla.

Kang, Y. C., Roh, H. S., Kim, E. J., and Park, H. D. (2003). Synthesis of Nanosize Gd_2O_3:Eu Phosphor Particles with High Luminescence Efficiency under Ultraviolet Light, *J. Electrochem. Soc.*, **150**, H93.

Li, Q., Gao, L., and Yan, D. (2000). The crystal structure and spectra of nano-scale YAG:Ce^{3+}, *Mater. Chem. Phys.*, **64**, 41.

Liu, H., He, D., and Shen, F. (2006). Luminescence properties of green-emitting phosphor (Ba1-x, Sr-x) (2) $SiO_4:Eu^{2+}$ for white LEDS, *J. Rare Earths*, **24**, 121.

Meltzer, R. S., Feofilov, S. P., Tissue, R., and Yuan, H. B. (1999). Dependence of fluorescence lifetimes of $Y_2O_3:Eu^{3+}$ nanoparticles on the surrounding medium, *Phys. Rev. B.*, **60**, R14012.

Mishra, K. C., Raukas, M., Marking, G., Chen, P., and Boolchand, P. (2005). Investigation of fluorescence degradation mechanism of hydrated $BaMgAl_{10}O_{17}:Eu^{2+}$ Phosphor, *J. Electrochem. Soc.*, **152**, H183.

Murakami, K. (1999). Phosphors for lamps, in: *Phosphor Handbook*, eds. S. Shionoya and W. M. Yen, CRC Press, Boca Raton, Fla.

Nag, A. and Kutty, T. R. N. (2000). Role of B2O3 on the phase stability and long phosphorescence of $SrA_{l2}O_4$:Eu, Dy, *J. Alloys Comp.*, **354**, 221.

Ninagawa, C., Yoshida, O., and Ashizaki, S. (1971). Japanese Patent (Kokoku) 46-17394.

Noyan, I. C., Shaw, T. M., and Goldsmith, C. C. (1997). Inhomogeneous strain states in sputter deposited tungsten thin films, *J. Appl. Phys.*, **82**, 4300.

Ohno, K. and Abe, T. (1986). Effect of BaF2 on the synthesis of the single-phase cubic $Y_3Al_5O_{12}$:Tb, *J. Electrochem. Soc.*, **133**(638), 525.

Park, J. K., Kim, C. H., Choi, K. J., Park, H. D., and Choi, S. Y. (2004). Effect of beta-stabilizing transition elements on elastic modulus of Ti-M systems, *Mater. Sci. Forum*, **449**, 952.

Peng, T., Yang, H., Pu, X., Hu, B., Jiang, Z., and Yan, C. (2004). Combustion synthesis and photoluminescence of $SrAl_2O_4$:Eu, Dy phosphor nanoparti, *Mater. Lett.*, **58**, 352.

Schlotter, P., Baur, J., Hielscher, C., Kunzer, M., Obloh, H., Schmidt, R., and Schnerder, J. (1999). Fabrication and characterization of GaN/InGaN/AlGaN double heterostructure LEDs and their application in luminescence conversion LEDs, *Mater. Sci. Eng. B.*, **59**, 390.

Silversmith, A. J., Boye, D. M., Brewer, K. S., Gillespie, C. E., Lu, Y., and Campbell, D. L. (2006). D-5(3) -> F-7(J) emission in terbium-doped sol-gel glasses, *J. Lumin.*, **121**, 14–20.

Smets, B., Rutten, J., Hoeks, G., and Verlijsdonk, J. (1989). $2SrO.3Al_2O_3$ Eu^{2+} and 1.29 (Ba, Ca)O, $6Al_2O_3$ Eu^{2+} – 2 new blue emitting phosphors, *J. Electrochem. Soc.*, **136**, 2119.

Steigerwald, D. A., Bhat, J. C., Collins, D., Fletcher, R. M., Holcomb, M. O., Ludowise, M. J., Martin, P. S., and Rudaz, S. L. (2002). Illumination with solid state lighting technology IEEE, *J. Sel. Top. Quantum Electron.*, **8**, 310.

Tsao, J. Y. (2002). *Light Emitting Diode (LEDs) for General Illumination*, 81, Optoelectronics Industry Development Association, Washingtons, D.C.

Wang, X.-J., He, Z. Y., Jia, D., Strek, W., Dariusz, R., Hreniak, D., and Yen, W. M. (2005). Crystal size dependence of the persistent phosphorescence in $Sr_2ZnSi_2O_7:Eu^{2+}$, Dy^{3+}, *Microelectron. J.*, **36**, 546.

Yang, P., Yao, G., and Lin, J. (2004). Energy transfer and photoluminescence of $BaMgAl_{10}O_{17}$ co-doped with Eu^{2+} and Mn^{2+}, *Opt. Mater.*, **26**, 327.

Ye, T., Guiwen, Z., Weiping Z., and Shangda, X. (1997). Combustion synthesis and photoluminescence of nanocrystalline Y_2O_3:Eu phosphors, *Mater. Res. Bull.*, **32**, 501.

Zhang, X., Liang, L., Zhang, J., and Su, Q. (2005). Luminescence properties of (Ca1?xSrx)-Se:Eu^{2+} phosphors for white LEDs application, *Mater. Lett.*, **59**, 749.